Structure of the Jahn-Teller distorted Cr^{2+} defect in SrF_2:Cr by electron-spin-echo envelope modulation

P. B. Oliete, V. M. Orera, and P. J. Alonso
Instituto de Ciencia de Materiales de Aragón, Universidad de Zaragoza-Consejo Superior de Investigaciones Científicas, Pza. San Francisco s/n, 50009 Zaragoza, Spain

(Received 27 March 1996; revised manuscript received 28 June 1996)

Electron spin echoes have been obtained by two-pulse ($\pi/2$-τ-π) and three-pulse ($\pi/2$-τ-$\pi/2$-T-$\pi/2$) experiments in the $|+1\rangle \leftrightarrow |-1\rangle$ EPR resonance transitions of the Jahn-Teller orthorhombically distorted Cr^{2+} in SrF_2:Cr. Particular emphasis is placed on the stimulated electron spin envelope modulation (ESEEM). Since this system has a spin $S=2$ and the zero-field-splitting contribution is of the same order of magnitude as the electronic Zeeman term, a new formalism for analysis of the ESEEM has been developed, allowing us to extend the Mims formalism for $S=1/2$ to more complex systems. Applying it to our results we have determined the superhyperfine (shf) interaction tensors of Cr^{2+} with the nearest-neighboring (NN), next-nearest-neighboring (NNN), and third-shell-neighboring fluoride ions, estimating the Cr^{2+}-F^- distances with the orthogonalized envelope function method. The defect model consists of four fluoride ions in the yz (110) defect plane which relax inwards to touch the Cr^{2+} ion. The remaining four fluoride ions relax outwards to fit into the next Sr^{2+} ions cage. [S0163-1829(96)00441-9]

I. INTRODUCTION

Electron-spin-echo envelope modulation (ESEEM) spectroscopy is a powerful technique to determine the structure of paramagnetic systems. It is a time-domain spectroscopy that can supply information on the nature and spatial arrangement of ligands providing they include some nuclei with nuclear magnetic momenta. The interaction of the electron paramagnetic system with the surrounding nuclei, the so-called superhyperfine (shf) interaction, can produce a time modulation on the electron-spin-echo (ESE) decay envelope. The frequency spectrum of this modulation can be associated with the small shf splitting of the resonance lines.[1–4]

Seen from this aspect, ESEEM spectroscopy gives information similar to that of electron-nuclear double resonance (ENDOR). However, in addition to being a time-domain spectroscopy which provides a direct measure of the relevant relaxation times, the intensity of the ESEEM does not depend on any magnetic relaxation rate as ENDOR, thus making it easier to detect in some cases. Furthermore ESEEM, at difference with ENDOR, is sensitive to very small splittings so that frequencies well below 1 MHz, the limit for conventional ENDOR, can be easily measured by ESEEM. High resolution in the frequency domain can also be achieved by ESEEM when the decay is analyzed by backwards linear prediction (BLP) methods.[5]

In the last few years, the technique has been extensively applied to the study of the structure of molecules in orientationally disordered solids but less often to that of ions or defects in ionic crystals.[6] The lack of research into single crystals can be explained by the difficulty in getting suitable systems. In fact, the most interesting systems to study are crystals having constituent ions with nonzero nuclear momenta. Unfortunately dipolar magnetic interactions between the paramagnetic electron and the matrix nuclear momenta shorten the spin-relaxation times. Due to the dead time of the ESE spectrometer in practice only systems with relaxation times larger than $\simeq$200 ns can be measured.[1] Thus there is an experimental limitation which does not allow the study of many interesting systems by this technique.

Echoes in inhomogeneously broadened EPR lines can be generated by the well-known two-pulse ($2p$) and three-pulse ($3p$) sequences. The $2p$ decay is governed by the phase memory relaxation time T_M whereas the spin-lattice relaxation time T_1 is the relevant time for $3p$ experiments. Since for crystals the latter is usually 1 order of magnitude longer than the former, $3p$ experiments are preferable in order to study ESEEM of ions and defects in single crystals. Moreover the frequency spectrum of the $3p$ echo decay is simpler than that of the $2p$ one.[1]

The fundamentals of the ESEEM phenomenon are well known for the simplest $S=1/2$, $I=1/2$ system.[1–7] ESEEM has also been used to study $S=1$,[8] $S=3/2$ and 5/2 (Refs. 9 and 10) systems with small zero-field splittings. In these cases the problem has been reduced to that of a spin-doublet leading to expressions for the echo intensity similar to these of the $S=1/2$ case. Less attention has been paid to the study of $S=2$ systems where recently only a few ENDOR or ESEEM studies have been made available.[11] However, the ESEEM theoretical treatment has only been developed in the case of very large zero-field-splitting (ZFS) terms and for the EPR transitions within the $|\pm 2\rangle$ non-Kramers' doublet. Again within this approximation the problem is straightforwardly reduced to that of a spin doublet that can be described in terms of a simple fictitious spin $S'=1/2$ with a Hamiltonian

$$\mathcal{H}=4g_{\parallel}\beta B_z S'_z+\Delta S'_x, \tag{1}$$

where Δ is the doublet splitting at $B_z=0$ and z is determined by the ZFS axial term. Unfortunately, if the ZFS terms are not very large, strong mixing between the states takes place and the treatment is, as we will see, more complex.

Recently some cw-EPR studies on the d^4 Cr^{2+} ion in fluorite crystals have been reported.[12–15] Since the ion configuration is non-Kramers, EPR is difficult to detect and the literature on conventional EPR studies is very scarce for this ion. Furthermore we have not found any previously advanced reported EPR studies until our recent work on the ESEEM associated to an impurity perturbed Cr^{2+} defect in CaF_2.[12] Using this technique we were able to determine the defect model and the tensor of the shf interaction with the two F^- surrounding nuclei for this defect.

Besides this perturbed Cr^{2+} defect the published results suggest that Cr^{2+} ion when isolated enters the fluorite structure in a Jahn-Teller (JT) distorted orthorhombic site in CaF_2,[12] SrF_2,[13] and CdF_2,[14] and in a tetragonally distorted site in BaF_2 and $SrCl_2$.[15] The dominant fine-structure term is in all cases the zero-field-splitting axial term, which even for X-band frequencies is not large enough for Eq. (1) to be applicable. Strong state mixing complicates the theoretical treatment of the spectra and computer diagonalization of the spin Hamiltonians describing the spin system is necessary in all these cases.

From cw-EPR measurements it is clear that Cr^{2+} distorts the fluoride coordination cube along a C_2 symmetry axis to produce the observed orthorhombic symmetry in CaF_2, SrF_2, and CdF_2. As discussed by Oliete *et al.*[12] such a distortion is compatible with the JT effect. In fact coupling of the $^5T_{2g}$ electronic ground state of the metal ion to both e_g and t_{2g} modes of the ML_8 (O_h symmetry) cubic cluster can produce orthorhombic distortions under certain conditions of quadratic coupling[16,17] and the minima correspond to environments with four equidistant fluoride ions in the (110) planes.

The study of the Cr^{2+} conventional EPR spectra gave valuable information about g and zero-field tensors and also the defect symmetry but it has not been able to throw any light on the positions of the distorted ligands. This information is very important in understanding the nature of the quite unusual orthorhombic JT systems. The reason for this failure is that the shf structure with the surrounding fluoride ions observed in some EPR resonance lines has not yet been well interpreted. Although the shf structure of Cr^{2+} in SrF_2 and CdF_2 has been eventually associated to a nearly isotropic shf interaction with the four nearest-neighboring (NN) crystallographycally equivalent fluoride ions,[13,14] the interpretation does not seem very clear as fluoride p orbitals should always give some anisotropic contribution to the shf interaction.

To elucidate this important point we have measured and interpreted the orientationally resolved ESEEM of Cr^{2+} in SrF_2. The results reported in this work are an illustrative example of a JT distorted ion studied by this technique. We have measured the ESE decay for transitions within the $|\pm1\rangle$ doublet which are the most intense in this case. The theoretical treatment for the ESEEM departs from the one previously used for other $S>1/2$ ions. shf interaction up to the third-neighbor shell has been resolved from the ESEEM experiments. The shf tensor principal values were analyzed by a linear combination of atomic orbitals (LCAO) method[18] to obtain the Cr^{2+}-F^- distances which has led us to propose a sensible yet somewhat unexpected defect model.

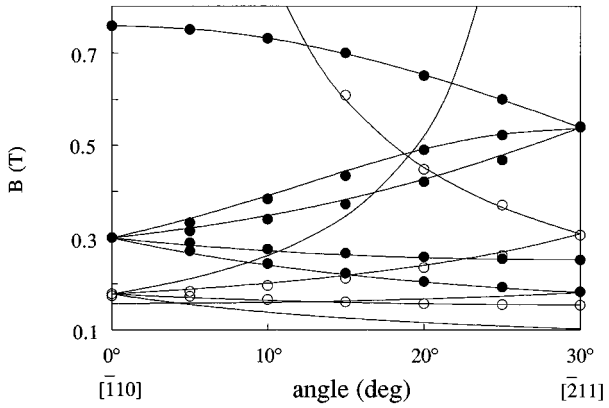

FIG. 1. The angular dependence of the EPR line positions of SrF_2:Cr^{2+} for a (111) plane measured at 10 K in the X band. The experimental points correspond to ○, $|+2\rangle\leftrightarrow|-2\rangle$ and ●, $|+1\rangle\leftrightarrow|-1\rangle$ transitions. Solid lines are the calculated line positions using Eq. (2) and the parameter values given in Table I.

II. EXPERIMENTAL DETAILS

Single crystals of SrF_2:Cr used in the present work were grown in our laboratory using a standard Bridgman method in an argon atmosphere and carbon crucibles. The CrF_3 content in the starting material was 0.5%. Samples were colorless.

cw-EPR in both the X- and Q-band and X-band ESE experiments were performed in a Bruker ESP380E spectrometer. Low-temperature measurements were taken using an Oxford CF 935 continuous-flow cryostat refrigerated with liquid He. A TWT tube was used as microwave amplifier in the ESE measurements. The width of the $\pi/2$ pulses was adjusted to 16 ns and the echo decay was sampled with a minimum time interval of 8 ns over 1024 point data. As stated in the text different experimental parameters were used in some cases. The intensity and phase of the microwave pulses were optimized by maximizing the ESE amplitude. Suitable phase cycling was performed to eliminate unwanted echoes.

The magnetic field values were determined with a NMR gaussmeter and the diphenylpicrylhydrazyl (DPPH) signal ($g=2.0037\pm0.0002$) for the Q band and a Hewlett-Packard microwave frequency counter 5350B for the X band was used to measure the microwave frequency.

III. EXPERIMENTAL RESULTS AND INTERPRETATION

A. cw-EPR

X- and Q-band EPR measurements on SrF_2:Cr crystals were performed as a function of the angle between the crystallographic axes and the external magnetic field **B** lying in the (110) and (111) planes at temperatures in the 4–40 K range. Figure 1 shows the orientational diagram for rotations in the (111) plane for 10 K at 9.7 GHz.

The angular dependence of the resonance line positions and intensities can be described by the following approximate spin Hamiltonian (SH) corresponding to an ion with an electronic spin $S=2$ in an orthorhombic symmetry that we ascribed to Cr^{2+}

TABLE I. Spin Hamiltonian parameters for Cr^{2+} in SrF_2. D, E, and a are given in cm^{-1}.

	g_x	g_y	g_z	D	$E-\frac{a}{6}$	$\lvert a\rvert$
This work	1.98(1)	1.99(1)	1.95(1)	−2.78(3)	0.0255(3)	0.030(7)
Ref. 13	1.96(1)	1.98(1)	1.94(1)	−2.791(3)	0.0283(2)	0.037

$$\mathcal{H}_0=\beta(g_xS_xB_x+g_yS_yB_y+g_zS_zB_z)+DS_z^2+E(S_x^2-S_y^2)+\frac{1}{6}a(S_1^4+S_2^4+S_3^4), \quad (2)$$

with $x=[\bar{1}10]$, $y=[001]$, and $z=[110]$.

In Eq. (2) the SH parameters have their usual meaning. In the cubic term, 1, 2, and 3 are the axes of the fluoride cube. The dominant fine-structure term is D, which produces a splitting of the fivefold degenerated state into a singlet $|0\rangle$ and two doublets $|\pm1\rangle$ and $|\pm2\rangle$. The transitions observed in our experiments are the $|+2\rangle\leftrightarrow|-2\rangle$ and $|+1\rangle\leftrightarrow|-1\rangle$ for both X and Q bands. The $|0\rangle\leftrightarrow|\pm1\rangle$ transitions were not detected because of experimental limitations in the magnetic field intensity. The states are named with their high field label.

The parameters obtained from the fitting of the calculated line positions using an exact diagonalization of the SH of Eq. (2) (given by solid lines in Fig. 1) to the experimental ones both for X and Q band are given in Table I.

With this set of parameters an excellent agreement between the observed and calculated line positions and intensities was obtained. The sign of D was determined using the temperature dependence of the line intensities, corresponding to the $|\pm2\rangle$ doublet as ground state. The intensity ratio between the $|+2\rangle\leftrightarrow|-2\rangle$ and the $|+1\rangle\leftrightarrow|-1\rangle$ transitions was used to obtain the $|a|$ value. The E value was determined with much uncertainty because it could not be obtained independently of the a value. So depending on the a sign two different E values that fit the experimental data were obtained. The SH parameters that we have obtained are very close to those recently given by Zaripov *et al.*[13] for Jahn-Teller distorted chromium ions in SrF_2 (see Table I), so we may assert that we are studying the same Cr^{2+} defect.

In our case, the shf spectrum corresponding to the $|+1\rangle\leftrightarrow|-1\rangle$ transition is only clearly resolved in some directions, the resonance lines being in general broad and structureless. Instead, for the $|+2\rangle\leftrightarrow|-2\rangle$ transition, the EPR lines present a shf-resolved structure consisting of five lines with an intensity ratio of 1:4:6:4:1 and an effective splitting of about 131 MHz for all the magnetic field orientations where they can be observed. A possible explanation is that a distribution in ZFS parameters, D and E, has little influence on the $|\pm2\rangle$ electronic energy splitting. Consequently for an $S=2$ spin system the $|+2\rangle\leftrightarrow|-2\rangle$ resonances are usually narrower than others and the shf structure can be better resolved in this case. The apparent isotropy of the shf structure leads to Zaripov *et al.*[13] to propose a shf interaction predominantly isotropic with four equivalent fluoride nuclei. In the following we will see if this interpretation is correct.

The shf structure caused by a shf interaction of the $3d$ Cr^{2+} electrons with four fluoride nuclei can be explained adding to the SH of Eq. (2) the following contribution:

$$\mathcal{H}_{\text{shf+nuc}}=\sum_{i=1}^{4}\{-g_n\beta_n\mathbf{I}^i\mathbf{B}+\mathbf{S}A^i\mathbf{I}^i\}, \quad (3)$$

which includes both nuclear Zeeman and superhyperfine interaction terms, to give

$$\mathcal{H}_{\text{fp}}=\mathcal{H}_0+\mathcal{H}_{\text{shf+nuc}}. \quad (4)$$

The eigenstates and eigenvalues of $\mathcal{H}_{\text{shf+nuc}}$ are obtained by applying perturbation methods up to first order using as zero-order states the eigenstates of $\mathcal{H}_0$. It comes out that the experimental data from the $|+1\rangle\leftrightarrow|-1\rangle$ transition are not enough to determine the unknowns in Eq. (3). On the other hand, a nearly isotropic shf structure in the $|+2\rangle\leftrightarrow|-2\rangle$ transition does not necessarily imply an isotropic shf interaction. In fact, for transitions within the $|\pm2\rangle$ non-Kramers doublet, the line positions can be predicted in a good degree of approximation by assuming that $\langle S_x\rangle\approx\langle S_y\rangle\approx0$ and $\langle S_z\rangle\approx\pm2$ depending on the spin variety considered. Then Eq. (3) becomes

$$\mathcal{H}_{\text{shf+nuc}}=\sum_{i=1}^{4}\{-g_n\beta_n(B_xI_x^i+B_yI_y^i+B_zI_z^i)+\langle S_z\rangle(A_{zx}^iI_x^i+A_{zy}^iI_y^i+A_{zz}^iI_z^i)\}, \quad (5)$$

with x, y, and z as the defect axes. The shf interaction is assumed to be axial, with x', y', and z' being the shf axes and z' along the Cr^{2+}-F^- bonding direction. For the relatively low magnetic fields where the $|+2\rangle\leftrightarrow|-2\rangle$ lines are observed, the nuclear Zeeman contribution is negligible when compared with the shf term, besides $\langle S_z\rangle$ is isotropic for this transition and so the shf structure given by Eq. (5) is nearly independent of the magnetic field orientation. This explains the apparent isotropy of the shf interaction observed for the $|+2\rangle\leftrightarrow|-2\rangle$ transitions. The relationship between the observed shf structure and the shf interaction parameters depends on the defect model used. If the z axis is perpendicular to the four-fluoride (110) plane, we can always choose $x'\|z$ and so $A_{zz}=A_\perp$, $A_{xz}=A_{yz}=0$. Then the eigenvalues of Eq. (5) are[12] $\lambda=\pm A_\perp$.

On the other hand, if the z axis is contained in the NN fluoride (110) plane then $x'\|x$ and $A_{xz}=0$, $A_{zz}=(\sin\theta)^2A_\perp+(\cos\theta)^2A_\|$ and $A_{yz}=\pm\sin\theta\cos\theta(A_\|-A_\perp)$, depending on the fluoride nucleus considered, θ being the angle between z' shf axis and the [110] direction. The eigenvalues in this case are given by

$$\lambda=\pm\{[(\sin\theta)^2A_\perp+(\cos\theta)^2A_\|]^2+[\cos\theta\,\sin\theta(A_\|-A_\perp)]^2\}^{1/2}. \quad (6)$$

So the defect model is far from being solved by conventional EPR experiments.

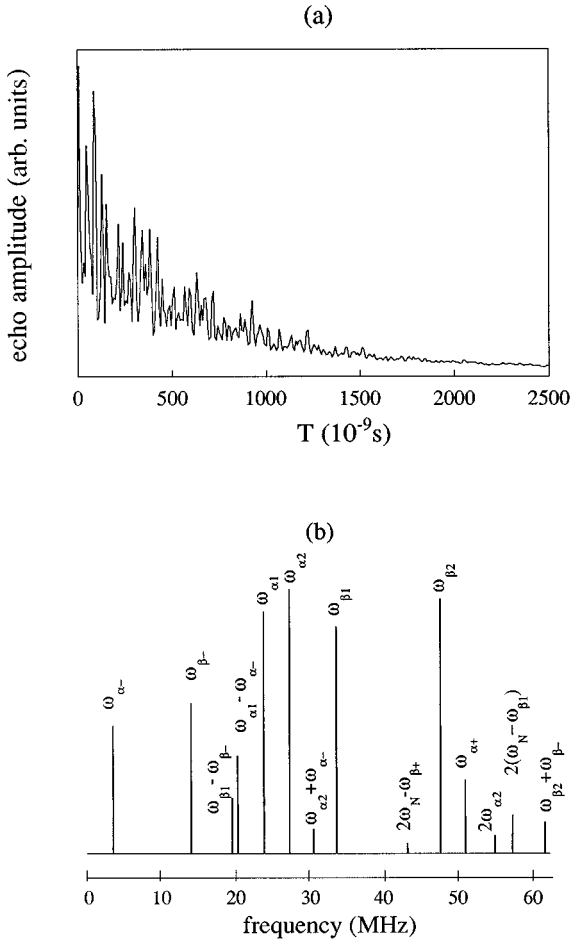

FIG. 2. (a) The ESE decay in a $3p$ experiment as a function of the time T between the second and the third pulses for the $z\|[101]$ center when the magnetic field is applied 70° away from the [001] direction in a (110) plane. The time origin has been displaced ≈300 ns to avoid uncompensated Mims echo contribution to the ESE signal. (b) The peaks obtained in the frequency domain of the previous decay using the BLP analysis method. [For labeling see text (Sec. III B).]

B. ESEEM

Two and three pulse experiments were performed in the X band in SrF_2:Cr crystals by rotating the magnetic field in the (110) and (111) planes at temperatures between 4 and 20 K. Electron spin echoes were only detected for the $|+1\rangle\leftrightarrow|-1\rangle$ transition. Attempts to observe ESE in the in the $|+2\rangle\leftrightarrow|-2\rangle$ transition failed presumably because of experimental limitations in the microwave power (see below). Typical decay times at 10 K were 0.5 to 1.2 μs, depending on the crystal orientation, for T_1 and ≈150 ns for T_M. As expected relaxation times shorten at higher temperatures and echoes are difficult to observe at temperatures above 20 K.

In Fig. 2(a) we present the decay at 10 K of the echo amplitude for a $3p$ experiment as a function of the time T between the second and the third pulse for the defect whose z axis is parallel to the [101] direction, with **B** contained in a (110) plane. The spin-echo decay is analyzed in the frequency domain using either the usual method of the fast fourier transform (FFT) or the alternative one of the backward linear prediction.[19,20] The frequency spectrum corresponding to this decay is given in Fig. 2(b).

To analyze the measured ESEEM we have to take into account in the first place that the ZFS terms are too large for perturbation methods to be applied. Although the $|\pm2\rangle$ states can be approximately treated as a separated non-Kramers doublet with the SH of Eq. (1), the $|\pm1\rangle$ states strongly mix among them and with the $|0\rangle$ state, depending on the magnetic-field orientation. As a consequence in this representation the 5×5 SH cannot be separated into two 2×2 and one 1×1 boxes. The electronic levels involved in the $|+1\rangle\leftrightarrow|-1\rangle$ EPR transition cannot be treated as an $S'=1/2$ system and consequently, Mims treatment is not directly applicable. Therefore we are currently looking for another strategy.

In a pulse experiment we have to distinguish successive periods of nutation and free precession. The evolution of the electron states during these time periods can be followed by means of the density-matrix formalism, where the equation of motion that predicts the evolution of the spin system under the influence of a spin Hamiltonian $\mathcal{H}(t)$, given in frequency units, in the defect axes frame is[21]

$$\frac{d\rho(t)}{dt}=i[\rho(t),\mathcal{H}(t)], \tag{7}$$

where $\rho(t)$ is the density-matrix operator of the system and

$$\mathcal{H}(t)=\mathcal{H}_{\rm fp}+\mathcal{H}_1(t), \tag{8}$$

with $\mathcal{H}_{\rm fp}$, the Hamiltonian defined in Eq. (4), and

$$\mathcal{H}_1(t)=2\mathcal{H}_1\cos\omega t=\mathcal{H}_1(e^{i\omega t}+e^{-i\omega t}) \tag{9}$$

for the interaction with the microwave field.[22] This last term introduces a time dependence on the spin Hamiltonian during the nutation periods which complicates the solution of Eq. (7).

Let us first consider the problem of an $S=2$ electron system in interaction with an $I=1/2$ nucleus. During the free precession period, where the microwave field is switched off, the Hamiltonian that determines the system evolution is $\mathcal{H}_{\rm fp}$. Since $\mathcal{H}_{\rm fp}$ is time independent in the laboratory frame Eq. (7) can be solved by an expression as

$$\rho(t')=e^{-i\mathcal{H}_{\rm fp}(t'-t)}\rho(t)e^{i\mathcal{H}_{\rm fp}(t'-t)}. \tag{10}$$

In the representation of $\mathcal{H}_{\rm fp}$ the matrix $e^{-i\mathcal{H}_{\rm fp}(t'-t)}$ is diagonal with elements $e^{-iE_{km}(t'-t)}$, E_{km} being the eigenenergies of $\mathcal{H}_{\rm fp}$. Since $\mathcal{H}_{\rm shf+nuc}\ll\mathcal{H}_0$, the eigenstates $|km\rangle$ in this representation can be obtained up to a good approximation degree by a first-order perturbation method over the $\mathcal{H}_0$ eigenstates. We define E_k,E_m and $|k\rangle$,$|m\rangle$ as the $\mathcal{H}_0$ and $\mathcal{H}_{\rm shf+nuc}$ eigenvalues and eigenstates, respectively, keeping in mind that the nuclear eigenvalues E_m and eigenstates $|m\rangle$ depend on the electronic spin variety labeled by k.

During the nutation period, when the microwave field is switched on, the Hamiltonian to be considered is $\mathcal{H}(t)$. Now Eq. (7) cannot be easily integrated because $\mathcal{H}(t)$ depends explicitly on time. In the standard ESEEM theory, when the electronic Zeeman Hamiltonian term is the dominant one, the solution of the dynamical equation is handled by restating the problem in a frame of reference rotating at the microwave frequency around the static magnetic field direction

(laboratory z axis). In this frame the time dependence of the microwave field is removed and the solution can be easily found.

If ZFS terms are dominant, passing to the reference frame of the microwave field places a time dependence on $\mathcal{H}_{\rm fp}$ which complicates the solution during the free precession time periods. To avoid this time dependence we have transformed both the Hamiltonians and the density-matrix equation of motion to the so-called ''interaction representation.'' We have proven that within this representation and if the excited EPR transitions do not share a common electronic spin level, the problem can be redefined in terms of a spin doublet leading to expressions for the primary and stimulated ESEEM which are formally similar to those given by the standard theory (see the Appendix A).

For a $3p$ sequence the time dependence of the stimulated echo intensity is given by Eq. (A12). Since the Cr^{2+} electrons are coupled to four fluoride nuclei the expression to be used is the one given by Dikanov,[1]

$$E_{\rm mod}(\tau,T)=\frac{1}{2}\left[\prod_{i=1}^{4}E_{i\alpha}(\tau,T)+\prod_{i=1}^{4}E_{i\beta}(\tau,T)\right], \quad (11)$$

where

$$E_{i\alpha}(\tau,T)=1-k_i/2[1-\cos(\omega_{i\beta}\tau)]\{1-\cos[\omega_{i\alpha}(\tau+T)]\}. \quad (12)$$

$E_{i\beta}(\tau,T)$ is obtained from Eq. (12) by permuting α and β. $k_i=4I_{ia}I_{if}$ is the modulation depth parameter, I_{ia} and I_{if} being the intensities of the allowed and forbidden EPR lines, respectively.

Here $\omega_{i\alpha}$ and $\omega_{i\beta}$ stand for the fundamental frequencies resulting from the interaction with the i nucleus in the α and β manifolds and among these the EPR transition occurs. These equations tell us that if there is a shf interaction with more than one nucleus all the possible combinations between shf frequencies belonging to the same electronic spin variety can also contribute to the $3p$ ESEEM pattern.

Using Eqs. (11) and (12), three different sets of frequencies have been identified corresponding to the interaction with the four nearest-neighboring (NN), the next-nearest-neighboring (NNN), and the third-shell neighboring fluoride ions. Figure 3 shows the dependence of the ESEEM frequencies on the orientation of the static magnetic field **B** for crystal rotation around a [110] crystallographic direction corresponding to the NN fluoride ions for the defect whose z axis is perpendicular to the rotation plane. Only two frequencies, ω_α and ω_β, are observed for this defect. In some directions, peaks corresponding to the $2\omega_\alpha$ combination are also detected. When the magnetic field is applied near the [110] direction, the echo modulation vanishes and no peaks are observed in this frequency domain.

The same experiments have been done for rotations in the (111) plane. The angular dependence of the ESEEM frequencies in both (110) and (111) planes can be explained with the defect model depicted in Fig. 4 and the Hamiltonian given in Eq. (4). The shf axes chosen here are x', y', and z' with x' parallel to the x defect axis and z' forming an angle θ with the [110] direction. In this model the four fluoride nuclei are placed in the (110) plane containing the defect z axis. The model is in contrast to previous ones where the defect z axis

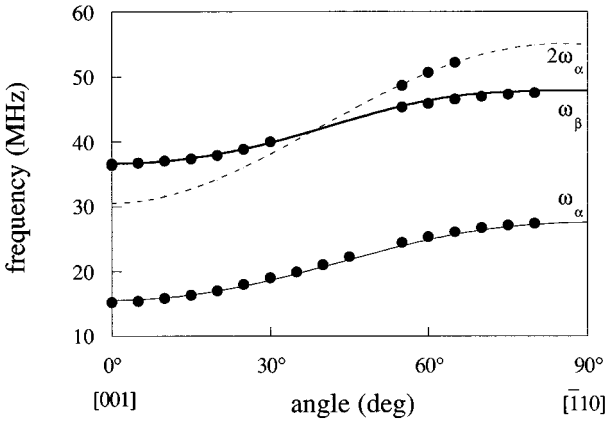

FIG. 3. The angular dependence of the peaks obtained for a $3p$ ESEEM experiment in a (110) plane for the defect whose z axis is perpendicular to the plane, measured at 9.8 GHz and 10 K. ω_α and ω_β correspond to the shf splittings in the up- and down-spin variety. The points correspond to the experimental frequencies and the lines to the calculated ones using Eq. (31) and the parameter values given in Table II.

was assumed to be perpendicular to the plane of nearest fluorides. ESEEM results univocally support this model. In fact if the magnetic field rotates in the (110) plane and for the defect whose z axis is parallel to [110], the shf interaction with the four fluoride nuclei is equivalent for all the directions contained in this plane. Due to this equivalency only two frequencies are expected, one for each electronic spin variety. If other defect configurations are considered, this equivalency is not kept and more frequencies should be observed. Figure 2(b) shows the ESEEM frequencies for a defect whose z axis is parallel to the [101] direction, when the magnetic field is applied at 70° from the [001] direction in the (110) plane. In this case the fluoride nuclei are equivalent in pairs and thus two different frequencies for each electronic spin manifold are detected, $\omega_{\alpha1}$, $\omega_{\alpha2}$ for the α electronic level and $\omega_{\beta1}$, $\omega_{\beta2}$ for the β electronic level. It can be also seen that most of the allowed frequency combinations predicted by Eq. (11) are detected too, for example $\omega_{\alpha\pm}=|\omega_{\alpha2}\pm\omega_{\alpha1}|$, $\omega_{\beta\pm}=|\omega_{\beta2}\pm\omega_{\beta1}|$. Those combinations

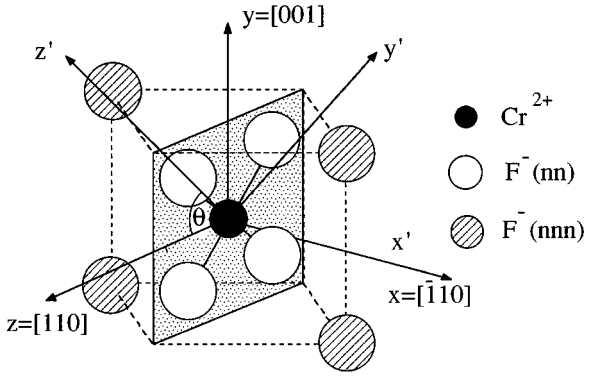

FIG. 4. The model for Cr^{2+} in SrF_2. x,y,z are the defect axes and x',y',z' the shf interaction axes for the NN fluoride nuclei. The NNN fluoride are also shown in the figure.

TABLE II. Superhyperfine Hamiltonian parameters for the three neighboring fluoride shells for Cr^{2+} in SrF_2, given in MHz.

	$A_\parallel$	$A_\perp$	θ (deg)	a	b
Shell 1	$+40\pm2$	$+17\pm1$	39 ± 5	24.7 ± 1.3	7.7 ± 1
Shell 2	$+12.5\pm2.5$	$+2\pm0.5$	35 ± 10	5.5 ± 0.7	3.5 ± 0.6
Shell 3	1.35	-0.7	65	0	0.67

which should appear at frequencies ω_c above the Nyquist frequency, ω_N (62.5 MHz for 8 ns sampling), are folded into $2\omega_N-\omega_c$.

The vanishing echo modulation amplitude in the $[\bar{1}10]$ direction can be explained in the frame of this model, since in this case the eigenstates of $\mathcal{H}_{\mathrm{shf+nuc}}$ corresponding to the two electronic levels involved in the transition coincide, the modulation depth parameter k_i goes to zero. For a model with defect z axis perpendicular to the NN fluoride plane this vanishing should not occur.

Once we have assigned all the peaks of the ESEEM frequency spectra either to an ENDOR frequency or to an allowed frequency combination we can fit the nuclear splittings calculated with the method outlined in Sec. III A to the experimental ones. The best fitting parameters, given by the principal values of the axial shf tensor $A_{x'x'}=A_{y'y'}=A_\perp$, and $A_{z'z'}=A_\parallel$, together with θ, the angle between the $Cr^{2+}-F^-$ bonding direction and the [110] crystal direction, are enumerated in Table II for the three studied coordination shells. The isotropic and anisotropic shf contributions defined as $a=(1/3)(A_\parallel+2A_\perp)$ and $b=(1/3)(A_\parallel-A_\perp)$, respectively, are also given in Table II.

The solid lines in Fig. 3 correspond to the theoretical shf splittings calculated with the Hamiltonian in Eq. (3) and the shf parameter values corresponding to the four first-neighboring fluoride ions. The relative intensities of the experimental ESEEM frequency spectrum are also approximately reproduced by the calculations.

For some orientations, apart from the lines associated to these four NN fluoride nuclei, other peaks at frequencies close to the Larmor frequency are detected. Figure 5 shows the angular dependence of these peaks obtained by the linear prediction method for rotations in a (110) plane and for the $z\|[011]$ defect. Two peaks can be clearly followed along all the rotational diagram. One of them corresponds to the fluorine Larmor frequency, ω_L, the other one at a higher frequency, is due to the shf interaction with the next-nearest-neighboring fluoride ions. Some combinations of this frequency with other ones corresponding to the NN shf interaction have been observed. All the combinations occur with shf splittings belonging to the down spin variety. In a $3p$ experiment only combinations between frequencies belonging to the same spin variety are allowed so we can univocally assign the shf splitting observed in the figure to the lowest spin electronic level.

The peak frequencies and the angular dependence can be interpreted as being due to the remaining four fluorides of the cube placed in the plane perpendicular to the z axis of the center (Fig. 4). The dashed lines in Fig. 5 correspond to the frequencies calculated with the parameters given for the second coordination shell in Table II, the two lowest ones being associated with the up electronic spin variety. In the experimental spectra some peaks with a lower intensity are observed in this region. Calculations predict such a low intensity for these peaks. Although their angular dependence qualitatively follows the prediction, they appear to be lower than 0.5 MHz below the calculated lines. We have tried to adjust both sets of lines to Eq. (3) but failed even using orthorhombic shf interaction tensors. We do not know at this stage where the origin for this small discrepancy lies.

Other peaks in the Larmor frequency region correspond to the third-shell neighbors (the fluoride ions placed in the six cubes adjacent to the Cr^{2+} fluoride cube). In fact, if we assume that these nuclei are fixed in their undistorted lattice sites and that the shf interaction is reduced to the dipolar anisotropic contribution, we can calculate their shf parameter values (see Table II). In the Fig. 5 we have plotted the splittings (solid lines) calculated with these parameter values, with i ranging from 1 to 24, following as before a perturbation method. Only those lines corresponding to the most intense predicted peaks are represented.

IV. DISCUSSION

The determination of the shf tensors has been done from the ESEEM detected on the $|+1\rangle\leftrightarrow|-1\rangle$ transitions. Well-resolved echoes are obtained when we perform either a well-optimized $2p$ or $3p$ experiment on these transitions. In the X- and Q-band cw-EPR spectra $|+2\rangle\leftrightarrow|-2\rangle$ transitions are

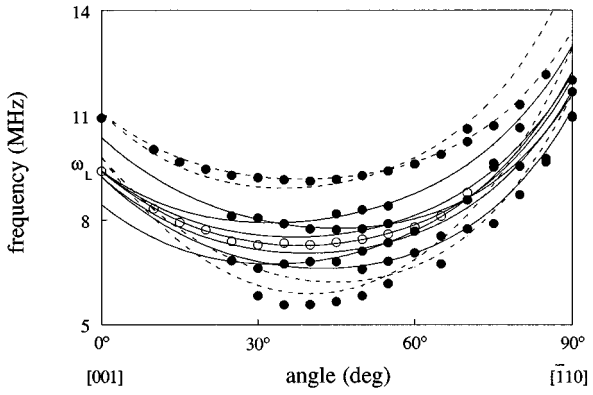

FIG. 5. The angular dependence of the shf frequencies (solid circles) near to the Larmor peak (open circles) obtained in a $3p$ experiment for the $z\|[011]$ defect at 7 K and 9.8 GHz by rotating the magnetic field in a (110) plane. Dashed lines are the calculated splittings for the NNN fluoride nuclei and solid lines for the third shell neighbors with the values given in Table II.

also observed, but attempts to detect ESE on these transitions failed. We interpret this failure as a consequence of the poorly optimized magnetization rotation as is explained below.

The fundamentals of the ESEEM phenomenon for an $S>1/2$ system with ZFS terms are developed in the Appendix. In particular in Eq. (A8) the effect of the exponential operators can be understood to produce rotations of the angle

$$\Theta = 2|\langle \alpha|\mathcal{H}_1|\beta\rangle| t_p \tag{13}$$

of the laboratory z component of the magnetization around the microwave magnetic field axis for an idealized square pulse of intensity B_1 and duration t_p. The echo intensity depends on this rotation angle, which also depends on the amplitude of the microwave transition between the electronic levels under consideration.

Using the eigenstates calculated from Eq. (2) we have estimated the matrix elements in Eq. (13) for both $|+1\rangle \leftrightarrow |-1\rangle$ and $|+2\rangle \leftrightarrow |-2\rangle$ transitions. Thus from optimized $2p$ and $3p$ $|+1\rangle \leftrightarrow |-1\rangle$ experiments we can predict the best experimental conditions for ESE on the $|+2\rangle \leftrightarrow |-2\rangle$ transition. Since the transition amplitude for the latter is much smaller than for the former by a factor of typically 6.6×10^{-2} either the microwave power, the pulse width, or both have to be increased. Limited microwave power from the generator used makes it necessary to increase the pulse width but since the $|+2\rangle \leftrightarrow |-2\rangle$ EPR signal is broad (typically about 300 MHz) this results in an incomplete excitation of the band, with the echo intensity decreasing when the pulse width increases. Thus a compromise between pulse intensity and width has to be found to obtain intense and well-defined echoes. Because of these constraints we have not been able to obtain an echo signal in the $|+2\rangle \leftrightarrow |-2\rangle$ transition.

Next we shall discuss the defect model. From cw-EPR results we know the orthorhombic symmetry of the defect and also that Cr^{2+} has four crystallographycally equivalent fluoride ions as nearest neighbors.

In principle, the orthorhombic symmetry is compatible with a JT distortion of the Cr^{2+} environment as was discussed in Ref. 12. So coupling of the metal ${}^5T_{2g}$ ground state with both e_g and t_{2g} cluster modes can produce orthorhombic distortions with potential minima for environments with four equidistant ligand ions in the (110) planes.[23] For this D_{2h} symmetry, two possible defect models can now be proposed. The center consists of a Cr^{2+} ion with four equidistant fluoride nuclei either in the (110) plane perpendicular to the defect z axis as it has been proposed for CaF_2:Cr (Ref. 12) and CdF_2:Cr (Ref. 14) or alternatively in the fluoride (110) plane containing the defect z axis.

The ESEEM results can only be interpreted when the defect z axis is in the (110) plane of the NN fluoride nuclei as has been previously established. Of course, with the shf parameters obtained from the ESEEM for the NN fluoride shell we predict from Eq. (6) a cw-EPR shf structure with a splitting of $4\lambda \approx 131$ MHz as observed. At this stage we believe that this can also be the case for JT distorted Cr^{2+} in CaF_2 and CdF_2. Unfortunately we did not detect ESE in CaF_2 presumably because of the short relaxation times and this hypothesis cannot be at present confirmed.

Besides the geometrical information from the angular dependence of the ESEEM, we have obtained the complete shf tensor for the four NN fluoride nuclei. We have analyzed these values using the orthogonalized envelope function method.[18] Within this frame the isotropic shf interaction constant is given by

$$a = \frac{8\pi}{3} g_e \mu_B g_n \mu_n \frac{1}{2S} \Sigma_i |\psi_s^i|^2, \tag{14}$$

where $\psi_{si}(R_i)$ is the i wave function of the LCAO involving the metal terms and the s orbitals of the ligand. The group-overlap integrals that contribute to ψ_{si} were calculated using the Clementi-Roetti atomic wave functions,[24] being dependent on the metal-ligand distance R_i. For the anisotropic contribution we have

$$b = g_e \mu_B g_n \mu_n \frac{1}{4S} \Sigma_i \int [(3\cos^2\theta - 1)/r^3] |\psi_{2p}^i(r)|^2 d\tau + b_{\text{dip}}, \tag{15}$$

where $\psi_{2pi}(r)$ is the i wave function of the LCAO involving the metal terms and the p orbitals of the ligand and b_{dip} (MHz) $=14.1549 g_n/R$ $(\text{Å})^3$ being the dipolar contribution. In our analysis only the three terms coming from the cubic ground state ${}^5T_{2g}$ were studied. Mixtures with the terms coming from the cubic ${}^5E_g$ and covalency effects were not considered here. To obtain the wave function of each term we followed a perturbative scheme from O_h to D_{4h} and then to D_{2h} symmetry, the ground states being A_g, B_{2g}, or B_{3g}.

Using the proposed defect model and Eqs. (14) and (15) we have calculated the a and b shf values as a function of the Cr^{2+} to ligand distance, R, for the three orbitals A_g, B_{2g}, and B_{3g}. Figure 6 shows the results of these calculations for both NN and NNN fluoride ions and compares them with the experimental values. The best fitting is obtained for a ${}^5A_g$ ground term, with $R_{\text{NN}} \approx 2.24$ Å for the nearest neighbors and $R_{\text{NNN}} \approx 2.62$ Å for the next-nearest neighbors. It is interesting to note that R_{NN} coincides with the sum of the Cr^{2+} and F^- ionic radii whereas R_{NNN} coincides with the expected Cr^{2+}-F^- distance if the NNN fluoride ions are displaced along the [111] direction until contact with the second shell Sr^{2+} cation. The geometrical configuration of this center tells us that by the effect of the JT distortion the fluoride cube distorts in such a way that four fluoride ions lying in a (110) plane relax inwards until they touch the smaller Cr^{2+} ion. The effect of the coupling to the e_g mode is reflected in their small departure from the cube [111] direction. The remaining four fluorides relax outwards from the central Cr^{2+} ion towards the ''cage'' produced by their nearest three Sr^{2+} ions. In this case the departure from the [111] direction is minimal due to the symmetry of the available space.

V. CONCLUSIONS

It has been proven that the formalism developed by Mims for the ESEEM of an $S=1/2$ system can be extended to any $S>1/2$ systems when the excited EPR transitions do not

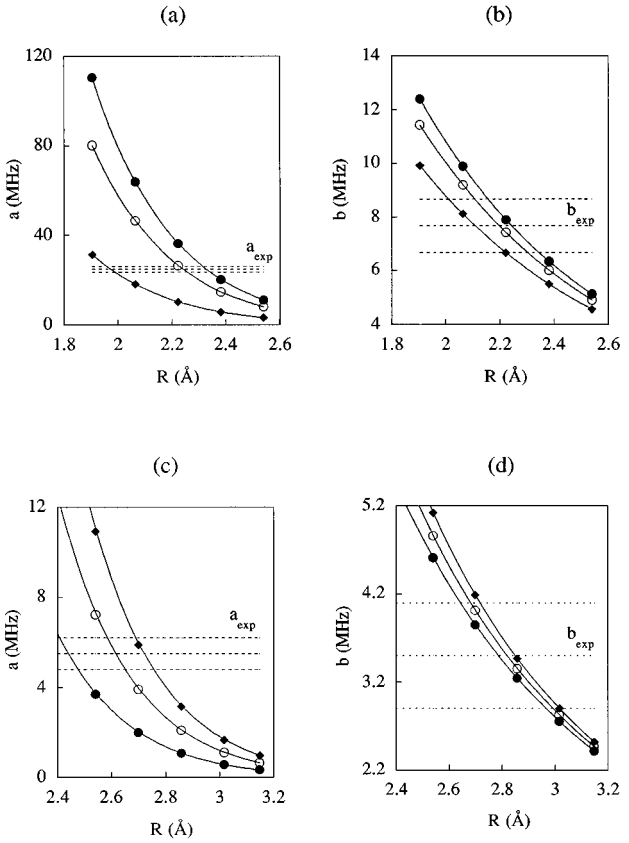

FIG. 6. (a) and (c) are the isotropic shf contributions for the NN and NNN fluoride nuclei, respectively, and (b) and (d) the corresponding anisotropic shf contributions calculated by the LCAO method as a function of the Cr^{2+}-F^{-} distance. Only the values for the terms coming from the cubic $^5T_{2g}$ are represented (○, A_g; ◆, B_{2g}; and ●, B_{3g}). The experimental a and b values with their errors are shown by dotted lines.

share a common electronic spin energy level. Electron spin echoes in the $|+1\rangle \leftrightarrow |-1\rangle$ transition of Cr^{2+} in SrF_2 were observed at temperatures below 20 K. By means of orientationally resolved ESEEM spectroscopy we have identified the fundamental nuclear frequencies associated with the shf interaction of an orthorhombically distorted Cr^{2+} with its three neighboring fluoride shells. The analysis of these frequencies and of their angular dependence allowed us to determine the shf tensors and from them, the geometrical model for this non-Kramers $S=2$ ion. Since the defect is not associated with any other impurities, the origin of the distortion is the Jahn-Teller effect.

ACKNOWLEDGMENTS

This research was sponsored by DGICYT under Contract No. PB 92-0040. One of us, P.B.O., would like to thank the Diputación General de Aragón for a grant.

APPENDIX

In this appendix, we will extend the conventional theory for the nuclear modulation of an $S=1/2$, $I=1/2$ spin system for two- and three-pulse ESE decay to the case of $S>1/2$ and relatively large ZFS terms. We will prove that for excited EPR transitions not sharing an electronic energy level the problem is reduced to that of a two-level system and the ESE decay is reproduced by the Mims equations.

Our task is to solve the dynamical Eq. (7) for the Hamiltonians given in Eqs. (4) and (8). For this purpose we will transform the operators ρ, $\mathcal{H}_{\rm fp}$, and $\mathcal{H}(t)$ in these equations with the canonical transformations given by the so-called ''interaction representation.'' Note that this is a different approach to that used in conventional ESEEM theories where transformation to the rotating frame is used instead. In the interaction representation the transformed operators are defined by

$$\rho^*(t)=e^{i\mathcal{H}_0 t}\rho(t)e^{-i\mathcal{H}_0 t}, \tag{A1}$$

$$\mathcal{H}_1^*(t)=e^{i\mathcal{H}_0 t}\mathcal{H}_1(t)e^{-i\mathcal{H}_0 t}. \tag{A2}$$

The Hamiltonians $\mathcal{H}_0$ and $\mathcal{H}_{\rm shf+nuc}$ are invariable under this transformation when the $\mathcal{H}_{\rm fp}$ representation $|km\rangle$ defined in Sec. III is adopted. The equation of motion that describes the evolution of the system during the nutation period is in this representation

$$\frac{d\rho^*(t)}{dt}=i[\rho^*(t),\mathcal{H}_{\rm shf+nuc}+\mathcal{H}_1^*(t)]. \tag{A3}$$

Now let us translate into this problem the arguments developed by Abragam when studying the broadening of EPR lines by dipole-dipole interactions.[25]

When the perturbative Hamiltonian $\mathcal{H}_{\rm shf+nuc}+\mathcal{H}_1^*(t)$ is absent $d\rho^*(t)/dt=0$, i.e., the density matrix $\rho^*(t)$ is independent with time. Then, if the perturbing Hamiltonian $\mathcal{H}_{\rm shf+nuc}+\mathcal{H}_1^*(t)$ is small (the microwave fields generated in the pulse spectrometer are less than 1 mT), the time evolution of $\rho^*(t)$ is expected to be slow. Using as a state basis that of $\mathcal{H}_{\rm fp}$ the matrix elements of Eq. (A3) are

$$-i\left\langle km\left|\frac{d\rho^*(t)}{dt}\right|ln\right\rangle=\langle km|[\rho^*(t),\mathcal{H}_{\rm shf+nuc}]|ln\rangle + \langle km|[\rho^*(t),\mathcal{H}_1^*(t)]|ln\rangle. \tag{A4}$$

Those matrix elements of $d\rho^*(t)/dt$ that vary rapidly with time are neglected. As $\mathcal{H}_{\rm shf+nuc}$ does not present any time dependence, the only term to be discussed is that involving $\mathcal{H}_1^*(t)$. We can develop the corresponding commutator in Eq. (A4) and use the definition (A2) to obtain

$$\langle km|[\rho^*(t),\mathcal{H}_1^*(t)]|ln\rangle=\langle km|\rho^*(t)\mathcal{H}_1^*(t)|ln\rangle-\langle km|\mathcal{H}_1^*(t)\rho^*(t)|ln\rangle$$

$$=\sum_{jp}\langle km|\rho^*(t)|jp\rangle\langle jp|\mathcal{H}_1^*(t)|ln\rangle-\sum_{jp}\langle km|\mathcal{H}_1^*(t)|jp\rangle\langle jp|\rho^*(t)|ln\rangle$$

$$=\sum_{jp}\langle km|\rho^*(t)|jp\rangle\langle jp|e^{i\mathcal{H}_0t}\mathcal{H}_1e^{-i\mathcal{H}_0t}|ln\rangle(e^{i\omega t}+e^{-i\omega t})-\sum_{jp}(e^{i\omega t}+e^{-i\omega t})$$

$$\times\langle km|e^{i\mathcal{H}_0t}\mathcal{H}_1e^{-i\mathcal{H}_0t}|jp\rangle\langle jp|\rho^*(t)|ln\rangle. \tag{A5}$$

As $|km\rangle$ are eigenstates of $\mathcal{H}_0$ with eigenenergies E_k we can write

$$\langle km|[\rho^*(t),\mathcal{H}_1^*(t)]|ln\rangle=\sum_{jp}(e^{i\omega t}+e^{-i\omega t})\langle km|\rho^*(t)|jp\rangle\langle jp|\mathcal{H}_1|ln\rangle e^{i(E_j-E_l)t}$$

$$-\sum_{jp}(e^{i\omega t}+e^{-i\omega t})e^{i(E_k-E_j)t}\langle km|\mathcal{H}_1|jp\rangle\langle jp|\rho^*(t)|ln\rangle. \tag{A6}$$

It follows that the only relevant terms that do not present any strong time dependence for $d\rho^*(t)/dt$ are those for which either $E_j-E_l\approx\pm\omega$ or $E_k-E_j\approx\pm\omega$. The other terms with fast varying time exponentials should be small and they can be neglected when compared with those involved in the EPR transition. This holds when some of the state pairs $\{|jp\rangle,|ln\rangle\}$ or $\{|km\rangle,|jp\rangle\}$ used to calculate the $\mathcal{H}_1$ matrix element are in resonance with the microwave field.

If there are only two such resonant states or better if adjacent transitions in the sense defined by Cofino *et al.*[10] are not simultaneously excited, the problem is reduced to that of a two-electron level system. For our experimental conditions only transitions within up to 6 mT are in resonance and contribute to the ESEEM.

In this study these are just the $|+1p\rangle$ and $|-1m\rangle$ states, α and β in the Mims notation.[7] The only elements of $\langle km|[\rho^*(t),\mathcal{H}_1^*(t)]|ln\rangle$ different from zero are those in which $|km\rangle$ and/or $|\mathrm{ln}\rangle$ coincide with α and/or β. Then the matrix elements $\langle km|[\rho^*(t),\mathcal{H}_1^*(t)]|ln\rangle$ can be written as $\langle km|[\rho^*(t),\mathcal{H}_1']|ln\rangle$, where $\mathcal{H}_1'$ is a time-independent Hamiltonian whose unique elements different from zero are $\langle\alpha|\mathcal{H}_1'|\beta\rangle=M\langle\alpha|\mathcal{H}_1|\beta\rangle$ with M the unitary matrix that relates the nuclear eigenstates of the α and β manifolds. In the notation adopted here the element $M_{mn}=\langle\alpha m|\beta n\rangle$. In this way we have obtained an effective Hamiltonian $\mathcal{H}_{\mathrm{shf+nuc}}+\mathcal{H}_1'$ over the two electronic manifolds involved in the EPR transition.

Equation (A3) can now be integrated because of the time independence of $\mathcal{H}_{\mathrm{shf+nuc}}+\mathcal{H}_1'$ obtaining as a solution for $\rho^*(t)$

$$\rho^*(t')=e^{-i(\mathcal{H}_{\mathrm{shf+nuc}}+\mathcal{H}_1')(t'-t)}\rho^*(t)e^{i(\mathcal{H}_{\mathrm{shf+nuc}}+\mathcal{H}_1')(t'-t)}. \tag{A7}$$

Due to the simple form of $\mathcal{H}_1'$ the problem can be reduced to the subspace generated by $|\alpha m\rangle$ and $|\beta n\rangle$. The analysis is simplified assuming $\mathcal{H}_{\mathrm{shf+nuc}}\ll\mathcal{H}_1'$, i.e., the microwave field amplitude is larger than the superhyperfine (shf) splittings and the pulse excites all the branching of transitions between $|\alpha m\rangle$ and $|\beta n\rangle$. Therefore during the nutation period

$$\rho^*(t')=e^{-i\mathcal{H}_1'(t'-t)}\rho^*(t)e^{i\mathcal{H}_1'(t'-t)} \tag{A8}$$

and during the free precession time the equation of motion (A3) with $\mathcal{H}_1^*(t)=0$ is solved to give

$$\rho^*(t)=e^{-i\mathcal{H}_{\mathrm{shf+nuc}}(t'-t)}\rho^*(t)e^{i\mathcal{H}_{\mathrm{shf+nuc}}(t'-t)}. \tag{A9}$$

The echo signal is given by $E(t)\propto\mathrm{Tr}\{\rho^*(t)\mathcal{H}_1^*(t)\}$. In the detection we only observe those terms which are time independent in the interaction representation. Terms oscillating at frequencies ω and 2ω can be ignored. Thus the echo signal is given by $E(t)\propto\mathrm{Tr}\{\rho^*(t)\mathcal{H}_1'\}$. $\rho^*(t)$ is calculated by applying Eqs. (A8) and (A9) to account for the successive nutation and free rotation periods, starting from the thermal equilibrium value

$$\rho_0=\frac{e^{-\mathcal{H}_{\mathrm{fp}}/kT}}{\mathrm{tr}\{e^{-\mathcal{H}_{\mathrm{fp}}/kT}\}}. \tag{A10}$$

Applying at this point the formalism developed by Mims[7] to the $2p$ and $3p$ sequences we straightforwardly obtain

$$E(\tau)=\sin\Theta_1(1-\cos\Theta_2)(|v|^4+|u|^4+|v|^2|u|^2[2\cos\omega_\alpha\tau+2\cos\omega\beta\tau-\cos\omega_+\tau-\cos\omega_-\tau]), \tag{A11}$$

$$E(\tau,T)=\sin\Theta_1\sin\Theta_2\sin\Theta_3\{|v|^4+|u|^4+|v|^2|u|^2[\cos\omega_\alpha\tau+\cos\omega_\beta\tau+(1-\cos\omega_\beta\tau)\cos\omega_\alpha(\tau+T)$$
$$+(1-\cos\omega_\alpha\tau)\cos\omega_\beta(\tau+T)]\}, \tag{A12}$$

with v and u the M elements as defined by Mims, allowed and forbidden transition amplitudes, τ the time interval between the first and the second pulses, T the time interval between the second and the third pulses, ω_α and ω_β the ENDOR splittings, $\omega_+=\omega_\alpha+\omega_\beta$, $\omega_-=|\omega_\alpha-\omega_\beta|$ and $\Theta_i=2|\langle\alpha|\mathcal{H}_1|\beta\rangle|t_{pi}$, t_{pi} being the i pulse width. Depending on the orientation considered the matrix element will be different, making it necessary to modify the microwave pulse power to maximize the ESE amplitude. The method we have followed is of general applicability to any case where electronic transitions excited by the width pulse do not share an electronic level.

[1] S. A. Dikanov and Y. D. Tsvetkov, *Electron Spin Echo Envelope Modulation (ESEEM) Spectroscopy* (CRC Press, Boca Raton, FL, 1992).

[2] L. Kevan, in *Time Domain Electron Spin Resonance*, edited by L. Kevan and R. N. Schwartz (Wiley, New York, 1979).

[3] L. G. Rowan, E. L. Hahn, and W. B. Mims, Phys. Rev. **137**, A61 (1965); **138**, 4 (1965).

[4] A. Schweiger, in *Modern Pulsed and Continuous-Wave Electron Spin Resonance*, edited by L. Kevan and M. Bowman (Wiley, New York, 1990).

[5] R. de Beer and D. Van Ormondt, in *Advanced EPR. Applications to Biology and Biochemistry*, edited by A. J. Hofft (Elsevier, New York, 1989).

[6] A. Schweiger, Angew. Chem. Int. Ed. Engl. **30**, 265 (1991).

[7] W. B. Mims, Phys. Rev. B **5**, 2409 (1972).

[8] D. J. Sloop, H. L. Yu, T. S. Lin, and S. I. Weissman, J. Chem. Phys. **75**, 3746 (1981).

[9] D. Grischkowsky and S. R. Hartmame, Phys. Rev. B **2**, 60 (1970).

[10] A. R. Coffino and J. Peisach, J. Chem. Phys. **97**, 3072 (1992).

[11] B. M. Hoffman, J. Phys. Chem. **98**, 11 657 (1994).

[12] P. B. Oliete, V. M. Orera, and P. J. Alonso, Phys. Rev. B **53**, 3047 (1996).

[13] M. M. Zaripov, V. F. Tarasov, V. A. Ulanov, G. S. Shakurov, and M. L. Popov, Phys. Solid State **37**, 437 (1995).

[14] R. Jablonsky, Mater. Res Bull. **8**, 909 (1973).

[15] P. B. Oliete, V. M. Orera, and P. J. Alonso, J. Phys. Condens. Matter **8**, 7179 (1996).

[16] P. J. Kirk, C. A. Bates, and J. L. Dunn, J. Phys. Condens. Matter **6**, 5465 (1994).

[17] C. A. Bates, Phys. Rep. **35**, 187 (1978).

[18] J. M. Spaeth, J. R. Niklas, and R. H. Bartram, *Structural Analysis of Point Defects in Solids*, Springer Series in Solid-State Sciences Vol. 43 (Springer, Berlin, 1992).

[19] H. Barkuijsen, R. de Beer, W. M. M. J. Bovée, and D. Van Ormondt, J. Magn. Reson. **61**, 465 (1985).

[20] H. Barkuijsen, R. de Beer, W. M. M. J. Bovée, and D. Van Ormondt, J. Magn. Reson. **64**, 343 (1987).

[21] C. P. Slichter, *Principles of Magnetic Resonance*, Springer Series in Solid-State Sciences Vol. 1, 3rd ed. (Springer, Berlin, 1990).

[22] In this case the tensor $\mathcal{H}_1$ as written in the defect axes frame cannot be easily decomposed into rotating and counter-rotating terms as usually done.

[23] C. A. Bates, J. L. Dunn, and E. Sigmund, J. Phys. C **20**, 1965 (1987).

[24] E. Clementi and C. Roetti, At. Data Nucl. Data Tables **14**, 177 (1974).

[25] A Abragam, *Principles of Nuclear Magnetism* (Oxford University Press, New York, 1961).